Elongational properties and crystallization of poly (isobutylene) melts probed by synchrotron radiation

A. Gonzalez-Alvarez* and M. Arellano
Departamento de Ingeniería Química, CUCEI, Universidad de Guadalajara,
Blvd. Marcelino García Barragán 1451, Guadalajara, Jal. 44430 MEXICO

O. Diat
European Synchrotron Radiation Facility BP 220, F-38043, Grenoble FRANCE

J.F. Legrand
UMR 585 (CEA-CNRS-Université Joseph Fourier)
DRFMC/CEA Grenoble 17 rue des Martyrs, 38054, Grenoble FRANCE

J.M. Piau
Laboratoire de Rhéologie, Université Joseph Fourier
Grenoble 1, Institut National Polytechnique de Grenoble, et
CNRS (UMR) 5520 Domaine Universitaire B. P. 53 F-38041 Grenoble, France Cedex 9

Recibido el 13 de enero de 2004; aceptado el 26 de abril de 2004

In this paper, we describe a phase transition in poly(isobutylene) of various molecular weight under elongational stress. Rheometry and wide angle X-ray diffraction have been performed simultaneously to correlate mechanical and structural properties of the material. The low molecular weight samples did not crystallize under the flow in the range of the strain rates applied. On the other hand, as the molecular weight increases the crystallization is always preceded by a strain of the samples under stretching.

Keywords: Elongational viscosity; crystallization; strain hardening; poly(isobutylene).

En este trabajo se describe la transición de fases de poliisobutileno de varios pesos moleculares sometidos a esfuerzos elongacionales. Experimentos de reometría y difracción de rayos X de ángulo amplio se realizan simultáneamente para correlacionar las propiedades mecánicas y la estructura del material. Muestras de polímero de bajo peso molecular no cristalizan en el intervalo de velocidades de deformación aplicadas. Al incrementar el peso molecular del polímero la cristalización obtenida es precedida por un endurecimiento del material debido a la deformación.

Descriptores: Viscosidad elongacional; cristalización; endurecimiento debido a la deformación; poliisobutileno.

PACS: 83.20.Hn

1. Introduction

One of the first papers about polymer crystallization under flow was published by van der Vegt and Smit [1]. They performed standard rheometrical measurements using a capillary rheometer for polyolefins (polypropylene, polyethylene and ethylene propylene copolymers) and natural rubber. Their studies were performed under stationary flow conditions at conventional processing temperatures (*i.e.* far above the melting point where the viscosity is lower) and also close to temperatures for which polymeric materials solidify. They observed that there exists a - temperature dependant- critical rate of flow at which the rheo-fluidification effect is replaced by a flow thickening effect (*i.e.* an increase of the apparent viscosity while increasing the rate of flow) and eventually a plugging of the capillary by crystallized polymer. The analysis of the X-ray diffraction pattern revealed a very high degree of orientation with a preferential **c** -axis parallel to the flow axis. van der Vegt and Smit interpreted this effect as a consequence of the flow-induced chain extension through the capillary. More recently Kolnaar and Keller [2] performed X-ray studies during the extrusion of a linear polyethylene. They found a temperature window, close to the melting point, where anomalous flow has been pointed out. They were able to relate this unusual behavior with the occurrence of a hexagonal crystalline phase which usually crystallizes into an orthorhombic structure.

Then it appears that there is a great interest to correlate precisely the structural studies of the polymer with its mechanical properties. Among polyolefins it is also well-known that Polyisobutylene (PIB) of high molecular weight may crystallize at room temperature under stretching. Therefore, PIB appears to be a good candidate for studying crystallization under elongational flow. The reasons are

i) PIB is a linear polymer (samples of different molecular weights and polydispersity are easy to dissolve in common solvents),

ii) PIB is not a semi-crystalline polymer at rest and at room temperature,

iii) it is easy to produce batch samples of different forms (rods, sheets), and

iv) PIB is not a mechanically degradable polymer.

Previous studies concerning the crystallization of PIB samples may be separated into two categories:

a Static studies on crystallized elongated samples.

b Real-time studies on the crystallization process.

In the first case, Brill and Halle [3], Fuller *et al.* [4], and Tanaka *et al.* [5] have determined the crystalline structure of PIB using stretched polymer samples of high molecular weight. They found a threshold deformation $L/L_o = 6$, where L_o is the initial length of the sample and L is the final length after stretching) for the onset of crystallization as well as the optimal stretching ratio ($L/L_o = 11$) to produce the best diffraction pattern. The structure determination has shown that crystalline PIB has a hexagonal unit cell and a chain conformation consisting of an $8/3$ helix with a periodicity $c = 18.63$ Å.

In the second case, Slonimsky *et al.* [6] have studied PIB samples stretched with a constant force and they identified three characteristic regimes in the strain variation as a function of time: the first one corresponds to the flow of the polymer in an amorphous state, the second one to the process of molecular ordering and crystallization, and the third one to the creeping flow regime in the crystalline state. The crystalline phase of the polymer in the latter regime was studied using X-ray diffraction techniques and electron-microscopic investigation of extended samples. When the tensile stress was released, the sample returned to the amorphous with the length close to its initial value. Later on, using a synchrotron beam, Koch *et al.* [7] conducted real time experiments with fibers of PIB. After a step deformation produced by a pneumatic driven piston, they were able to observe the onset of crystallization of the material with a short delay due to some relaxation process. But here again, the crystalline regions of the polymer melted immediately when elongational stress was released.

The aim of our work is to combine rheological measurements with an investigation of the possible phase changes under the elongational flow. For this purpose we constructed a new traction machine that can be mounted either on laboratory X-ray generators and on Synchrotron beam lines. The objectives were to study in real time the crystallization process of PIB samples, the structure and the orientation of the crystals as a function of the molecular weight, and the deformation rate. Indeed for low molecular weight samples the reptation time becomes smaller than the time scale of the experiment and then no crystallization is expected. In the next parts, we present and explain the rheological measurements, the X-ray diffraction experiments and finally the relationships between them.

2. Experimental

2.1. Materials

A series of PIB samples of different molecular weights and polydispersities were provided by BASF and Exxon. The values of M_w and M_w/M_n for the samples from BASF are listed in Table I. For the polymer L-140 from Exxon, the method of gel permeation chromatography was used to determine M_w/M_n and the results obtained by two different groups are given in the Table II.

TABLE I. Characteristics of PIB Oppanol samples (BASF 1989)

Polymer (Oppanol)	$M_w\ 10^3$ (gr/mol)	$M_n\ 10^3$ (gr/mol)	M_w/M_n
B10	36.5 – 45.0	22.0 – 25.0	1.66 – 1.80
B15	85.8 – 101.0	39.0 – 43.5	2.20 – 2.32
B100	1084 – 1491	218 – 271	4.97 – 5.50
B200	3960 – 5300	527 – 642	7.51 – 8.55

TABLE II. Characteristics of PIB L-140 sample.

Polymer (PIB L-140) Exxon	$M_w\ 10^3$ (gr/mol)	$M_n\ 10^3$ (gr/mol)	$\frac{M_w}{M_n}$
Hudson and Ferguson [10]	1 176 228	588 097	2
Willenbacher and Hingmann [11]	2 670 000	530 000	5

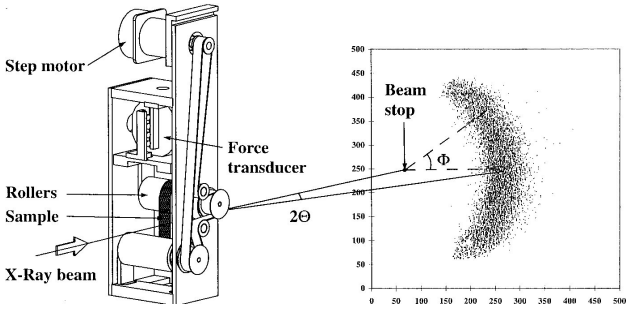

FIGURE 1. Sketch of the traction machine and of the initial scattering pattern recorded on a 2-D gas-filled detector at the ESRF. Before elongation the scattering of the polymer sample is isotropic and only a sector of the amorphous ring is recorded by the detector (2θ is the scattering angle and Φ is the azimuthal angle).

2.2. Sample preparation

For the low molecular weight PIB-polymers (B10 and B15), we prepared rod-like samples with 10 mm of diameter for B10 and 5 mm in diameter for B15. For high molecular weight PIB samples (B100, B200 and L-140), the polymer was dissolved in trichloroethylene and cast onto aluminium foils. After a total evaporation of the solvent, the polymer films were cut into rectangular sheets of $80 \times 28 \times 0.5$ mm^3 and glued on both ends on the rollers of the traction machine.

2.3. Traction machine

The components of the traction machine (see Fig. 1) are

i) two rollers with rough surfaces which can rotate with a constant speed,

ii) a stepping motor with a reduction gear, and

iii) a force transducer limited to 5N.

The general principles of the machine [8] are similar to the most basic rotary clamps rheometers developed by Meissner *et al.* [9]. Both rollers have the same linear velocity V. The length of the sample L_o being constant (L_o, defined as the distance between roller axis), the elongational strain rate is constant:

$$\dot{\varepsilon}_o = 2V/L_o \tag{1}$$

At the beginning of an experiment, the initial section S_o of the polymer sample is measured accurately for the calculation of the initial stress. Then, according to homogeneous strain assumption [8] we consider that the section sample decreases exponentially as a function of time,

$$S = S_o \exp(-2Vt/L_o) \tag{2}$$

where t is the elapsed time after start. This assumption is valid as long as the sample flows, but certainly inappropriate to describe the creeping of the crystalline sample. Nevertheless, to calculate transient stress we will use the above definition keeping in mind that the absolute values are different after the onset of the crystallization. Thus, the transient stress $\sigma(t)$ and the elongational viscosity η_E^+ can be written as follow:

$$\sigma(t) = F(t)\exp(2Vt/L_o)/S_o \tag{3}$$

$$\eta_E^+ = \sigma(t)/\dot{\varepsilon}_o \tag{4}$$

where $F(t)$ is the transient elongational force and it is recorded through the transducer during the experiment. In the following sections we will use the Hencky deformation $\dot{\varepsilon} = \ln(L/L_o)$ which in these experiments is given by:

$$\dot{\varepsilon} = \dot{\varepsilon}_o t \tag{5}$$

In general, for polymer melts under elongational flow, there exist two regimes. At low elongation rate, which corresponds to a Newtonian flow, it has been demonstrated that the elongational viscosity is equal to three times the transient shear viscosity ($\eta_E^+ = 3\eta^+$, the Trouton relationship). At high elongation rate, the flow behavior deviates from the Newtonian regime and an abrupt increase in the elongational viscosity called strain hardening has been frequently observed.

2.4. X-Ray diffraction set-up

The first X-ray diffraction experiments were performed using $CuK\alpha$ radiation from a classical generator. The measurements were performed using a Siemens powder diffractometer in transmission geometry. In order to follow the evolution of the diffracted intensity, a point detector mounted on a 2θ-arm was positioned at a fixed angle in the equatorial plane corresponding to the first Bragg reflection of the stretched sample.

In a second stage, real-time wide angle X-ray diffraction (WAXD) experiments were performed on the D24 beamline at LURE (the French Synchrotron facility in Orsay). The radiation was monochromatized to a wavelength $\lambda = 1.54$ Å, with an energy resolution ($\Delta\lambda/\lambda$ of 0.1 %). A one-dimensional position sensitive detector was placed horizontally at 180 mm from the specimen in order to detect the equatorial Bragg reflections between $2\theta = 10°$ and $2\theta = 28°$ (where 2θ is the scattering angle). Minimum time frame was reduced to 0.5 s.

In order to get more quantitative information on the line-shape of the Bragg peak, a series of experiments were performed at the European Synchrotron Radiation Facility (ESRF) in Grenoble on the high brilliance beamline (ID2). The ondulator gap as well as the Si 111 channel-cut monochromator were set in order to select a wavelength $\lambda = 0.75$ Åwith $\Delta\lambda/\lambda = 0.03\%$. A two-dimensional gas-filled detector with a spatial resolution of 600 μm was used and time frames were reduced to 0.1 s. It was positioned at 70 cm from the sample to cover Bragg angles from 3 to 11° (see Fig. 1). In order to get a fine correlation between the crystallization process and the rheological measurements the traction machine and the image acquisition were synchronized. All the experiments were performed at room temperature (22°C).

3. Results and discussion

3.1. Rheological measurements

The first evidence for a possible change of the polymer chain conformation is given by the evolution of the elongational

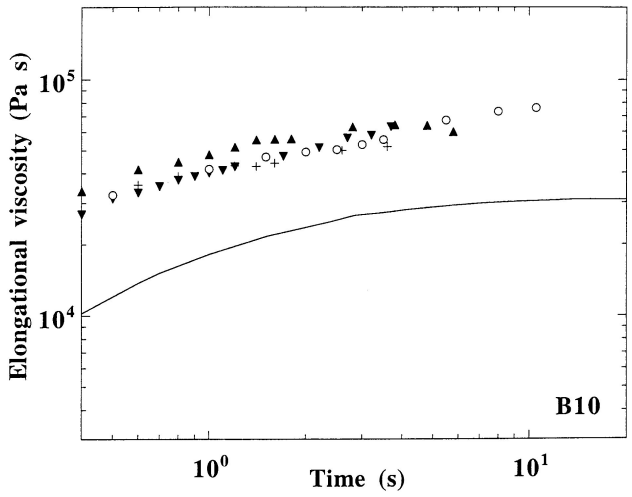

FIGURE 2. Real-time studies on the crystallization process for B10: $\circ, \dot{\varepsilon}_o = 0.11s^{-1}$; $\blacktriangle, \dot{\varepsilon}_o = 0.19s^{-1}$; $+$, $\dot{\varepsilon}_o = 0.38s^{-1}$; $\blacktriangledown, \dot{\varepsilon}_o = 0.47s^{-1}$. The solid line corresponding to the transient shear viscosity η^+ is displayed in order to be compared with the elongational viscosity (Trouton relation).

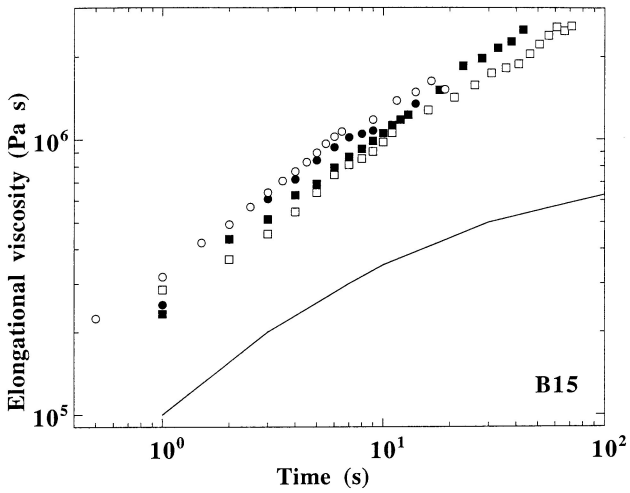

FIGURE 3. Real-time studies on the crystallization process for B15: $\square, \dot{\varepsilon}_o = 0.029s^{-1}$; $\blacksquare, \dot{\varepsilon}_o = 0.047s^{-1}$; $\circ, \dot{\varepsilon}_o = 0.095s^{-1}$; $\bullet, \dot{\varepsilon}_o = 0.11s^{-1}$. The solid curve is still a guide line for the corresponding transient viscosity and allows the reader to see a clear deviation of the elongational viscosity from the Newtonian behavior.

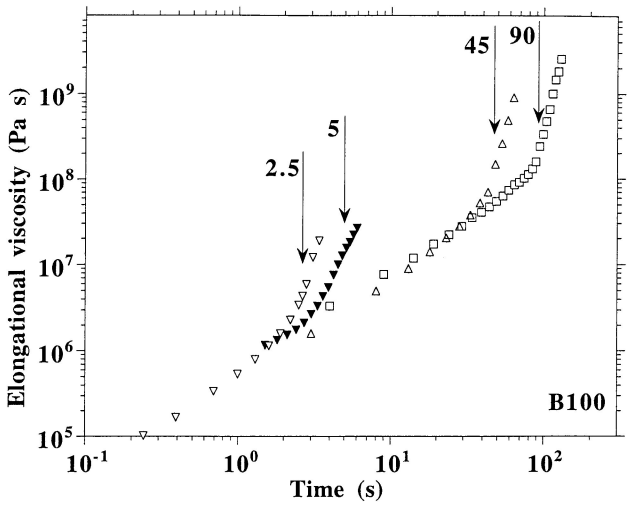

FIGURE 4. Real-time studies on the crystallization process for B100: $\square, \dot{\varepsilon}_o = 0.029s^{-1}$; $\triangle, \dot{\varepsilon}_o = 0.059s^{-1}$; $\blacktriangledown, \dot{\varepsilon}_o = 0.47s^{-1}$; $\triangledown, \dot{\varepsilon}_o = 0.95s^{-1}$.

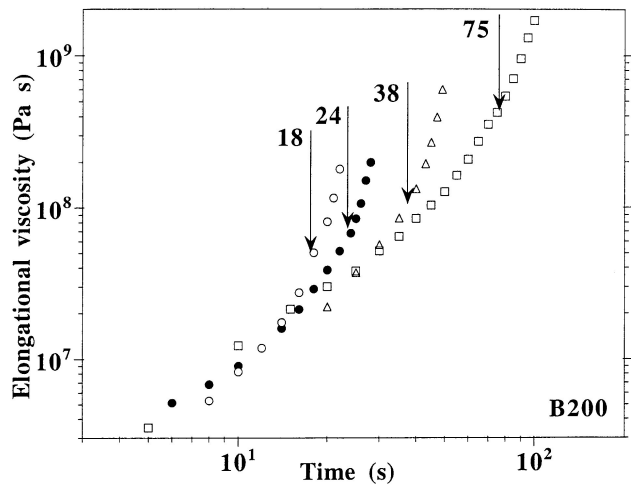

FIGURE 5. Real-time studies on the crystallization process for B200: $\square, \dot{\varepsilon}_o = 0.029s^{-1}$; $\triangle, \dot{\varepsilon}_o = 0.059s^{-1}$; $\bullet, \dot{\varepsilon}_o = 0.095s^{-1}$; $\circ, \dot{\varepsilon}_o = 0.11s^{-1}$.

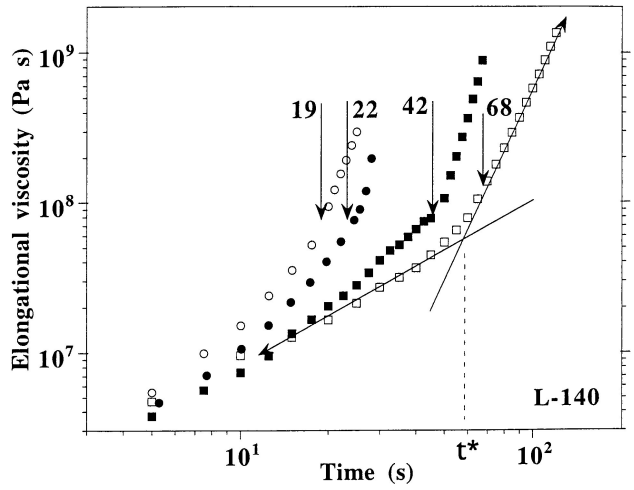

FIGURE 6. Real-time studies on the crystallization process for L-140: $\square, \dot{\varepsilon}_o = 0.029s^{-1}$; $\blacksquare, \dot{\varepsilon}_o = 0.047s^{-1}$; $\bullet, \dot{\varepsilon}_o = 0.38s^{-1}$; $\circ, \dot{\varepsilon}_o = 0.47s^{-1}$. The arrows in the graphs 4, 5 and 6 indicate the onset of crystallization determined from X-ray scattering experiments discussed in the next sections. The attached numbers correspond to t_c in seconds.

force as a function of time. Using the Eqs. (1)-(4), we can deduce and plot the variation the elongational viscosity η_E^+ as a function of time. In Figs. 2 – 6 we compare five samples of different molecular weights under different elongation rates. From these curves we observe a clear distinction between two groups of samples: the low molecular weight samples, B10 and B15 (Figs. 2, 3 respectively), for which no crystallization was observed for the elongation rates used and higher molecular weight samples B100, B200 and L-140 (Figs. 4, 5 and 6 respectively), which crystallize under elongational stress.

For the sample B10 these experiments were performed at strain rates from 0.11 to $0.47s^{-1}$. We essentially observe a Newtonian behavior and the transient elongational viscosity is approximately three times the transient shear viscosity [10] (Trouton relation). In contrast for the B15 sample we found the onset the strain hardening after 10 s (Fig. 3) when the transient elongational viscosity starts to deviate from the Newtonian behavior.

On the other hand, for the higher molecular weight PIB samples (second group) B100, B200 and L-140, one can notice two non-Newtonian regimes. In a first stage, these three samples exhibit a similar evolution - a strain hardening - and after a few seconds one observes an anomalous increase of the elongational viscosity corresponding to a divergence of the recorded elongational force. Such a behavior can also be seen in the results reported by Meissner [9] for polyethylene above its melting temperature. At short times, for the high molecular weight samples, the elongational viscosity has the

same magnitude whatever the strain rates; the strain hardening is observed until a stronger and an anomalous hardening occurs at time t^*, which depends on the strain rate. This time t^* corresponds to a change of slope in the $Log - Log$ plots and thus a change in the power law behavior of the viscosity. The two straight lines in Fig. 6 show how the value of t^* can be estimated. These values are listed in Table III. They suggest a renormalization of the curves with the strain rate $\dot{\varepsilon}_o$. Thus, using the Eqs. (3) and (5), the elongational stress at constant strain rate is plotted as a function of strain (see Figs. 7-9). It appears that almost all the curves show a unique behavior with these two regimes. Accordingly, it is found that the elongational stress depends on the strain rather than on the strain rate. The change of slope appears for the strain $\dot{\varepsilon}^* = \dot{\varepsilon}_o t^*$ whose estimated values are also given in Table III.

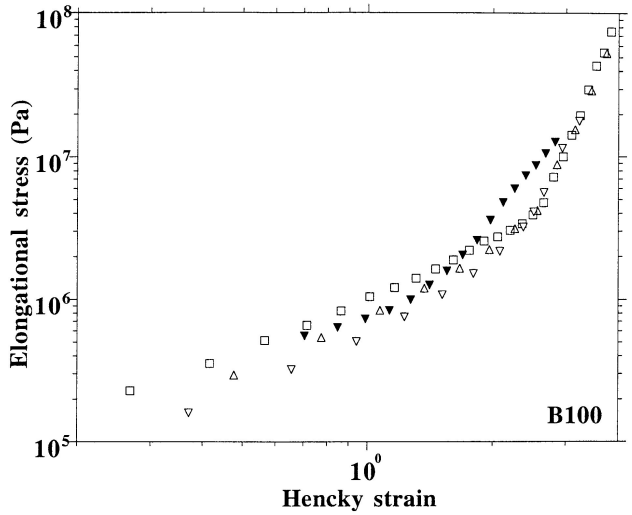

FIGURE 7. Same data are plotted in different coordinates: transient elongational stress $\sigma(t)$ versus Hencky strain $\dot{\varepsilon}$, only for samples showing crystallization under elongational stress B100.

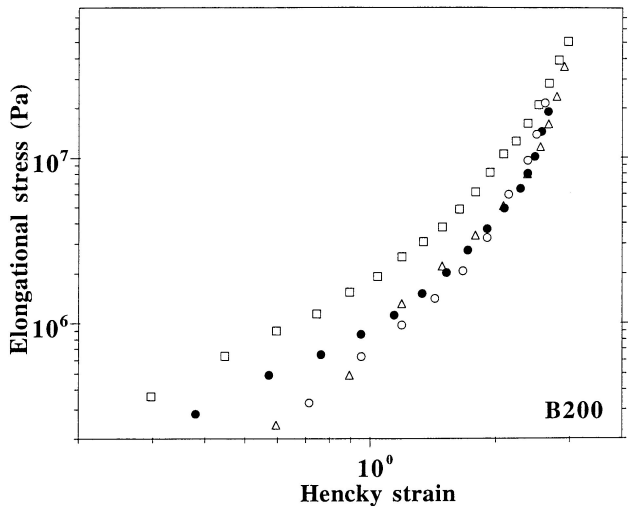

FIGURE 8. Same data are plotted in different coordinates: transient elongational stress $\sigma(t)$ versus Hencky strain $\dot{\varepsilon}$, only for samples showing crystallization under elongational stress B200.

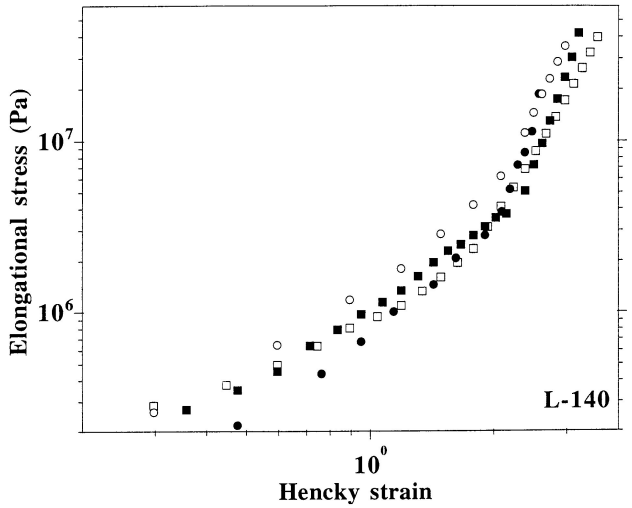

FIGURE 9. Same data are plotted in different coordinates: transient elongational stress $\sigma(t)$ versus Hencky strain $\dot{\varepsilon}$, only for samples showing crystallization under elongational stress L-140.

3.2. X-ray diffraction measurements

Having obtained the mechanical response of the PIB samples for different elongational rates as a function of time, the next step was to record simultaneously the scattering pattern and the elongational force in order to explore the possible coincidence between strain hardening and crystallization process. The X-ray diffraction and rheological measurements were carried out only on high molecular weight samples, which exhibit anomalous hardening (B100, B200 and L-140).

In some preliminary investigations, the traction machine was installed on a classical X-ray diffractometer, and powder diffractograms were recorded before and after elongation. The results obtained with the L-140 sample are displayed in Fig. 10. The scattering profile from the cast polymer film corresponds to the typical scattering pattern of an amorphous polymer; the broad peak is attributed to short range chain correlation [13]. In contrast, when the PIB sample is stretched, the diffraction pattern shows a sharp peak with a maximum intensity at $2\theta = 14.2$ deg. This is the composite $(020) + (110)$ Bragg peak in the equatorial plane of the stretched sample [5]. For the simultaneous measurements, we investigated samples of B200 with the X-ray detector positioned $2\theta = 14.2$ deg. Figure 11 displays the scattered intensity and the elongational viscosity as a function of time during stretching of B200 at a constant strain rate $\dot{\varepsilon}_o = 0.029\ \mathrm{s}^{-1}$. Initially, the scattered intensity decreases (due to the decrease of the sample cross section under elongation), and in the latter stage the intensity increases (due to an increase of the Bragg reflection from the crystalline regions that we define as "the crystallization process"). Finally it reaches a plateau. The time at which the intensity abruptly increases ($t = t_c$) corresponds to "the onset of crystallization". In this case, we emphasize that the variation of the scattered intensity at t_c is more abrupt than the change of slope observed at t^* in the elongational viscosity. During the

TABLE III. Results concerning the time slope change $-t^*-$ and the onset of crystallization $-t_c-$ for PIB samples.

	B100				B200				L-140			
$\dot{\varepsilon}_o(s^{-1})$	$t^*(s)$	$t_c(s)$	$\dot{\varepsilon}^*$	$\dot{\varepsilon}_c$	$t^*(s)$	$t_c(s)$	$\dot{\varepsilon}^*$	$\dot{\varepsilon}_c$	$t^*(s)$	$t_c(s)$	$\dot{\varepsilon}^*$	$\dot{\varepsilon}_c$
0.029	85	90	2.47	2.65	60	75	1.74	2.27	58	68	1.68	1.972
0.047	–	–	–	–	–	47.5	–	2.26	48	42	2.2	1.974
0.059	39	45	2.3	2.66	39	38	2.3	2.25	–	35	–	2.06
0.095	–	–	–	–	22	24	2.1	2.28	19	22	1.8	2.09
0.118	–	–	–	–	17	18	2.0	2.13	16	19	1.9	2.09
0.190	–	–	–	–	–	–	–	–	–	11	–	2.09
0.230	–	–	–	–	–	–	–	–	–	9	–	2.07
0.380	–	5.75	–	2.185	–	–	–	–	–	5	–	1.9
0.470	–	5	–	2.35	–	–	–	–	–	–	–	–
0.950	2.1	2.5	2.0	2.37	–	–	–	–	–	–	–	–
1.900	–	1.15	–	2.185	–	–	–	–	–	–	–	–
Average	–	–	2.25	2.32	–	–	2.04	2.24	–	–	1.90	2.03

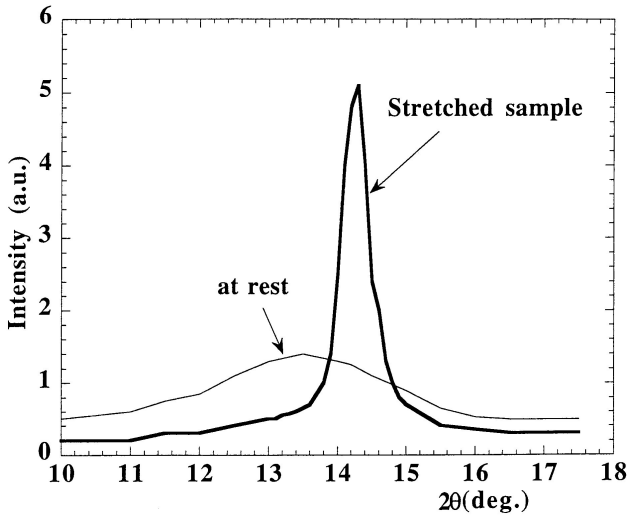

FIGURE 10. X-ray scattering curves of the L-140 sample at the initial state and after stretching obtained on a classical diffractometer (0-dimentional detector mounted on a 2θ-arm). These two curves show a first evidence of a phase change induced by the elongational flow. At rest the scattering curve corresponds to the typical diffractogram of an amorphous polymer, while in stretched sample a Bragg peak is detected at $2\theta = 14.2$ deg.

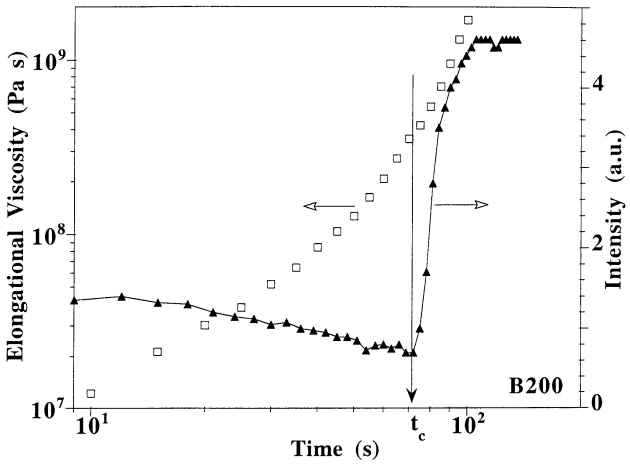

FIGURE 11. Plots of the elongational viscosity and the scattering intensity at the Bragg peak position, recorded simultaneously as the function of the time, for PIB B200 at $\dot{\varepsilon}_o = 0.029s^{-1}$, t_c corresponds to the time for which we observe the onset of crystallization under elongational flow.

crystallization process, the viscosity of the sample further increases and eventually diverges while the diffracted intensity increases. At the final stage, the intensity levels off indicating a maximum of the degree of crystallinity. Simultaneously, the deformation rate in the sample zone studied actually goes to zero because the sample exhibits a high (static) Young modulus. Thus it becomes impossible to measure a viscosity.

The experiments with a classical X-ray source were limited to a maximum strain rate $\dot{\varepsilon}_o = 0.118s^{-1}$, and data acquisition was limited. So further investigations were performed using a synchrotron radiation beam whose high flux also permitted to record Bragg reflection profiles during fast strain rates to obtain data more easily and to decide whether t_c coincides with t^*.

At LURE, scattering in the equatorial plane was recorded using a linear Position Sensitive Detector (PSD) covering the angular range 10 deg.$< 2\theta < 28$ deg. The evolution of the scattering pattern during elongation of L-140 is displayed in Fig. 12. Figure 12a shows the evolution of the intensity in function of elongation time and 2θ. For a strain rate of 0.047 s^{-1} we used a time frame of 4 second and the onset of crystallization was observed in the eleventh frame (*i.e.* 40 s$< t_c <$ 44 s). These experiments allowed us to determine more accurately the onset of crystallization at various elongational rates for B100 and L-140 (see Table III). In Fig. 12b, we show the evolution of the intensity as a function of 2θ for a few frames only, in order to extract the line width of the

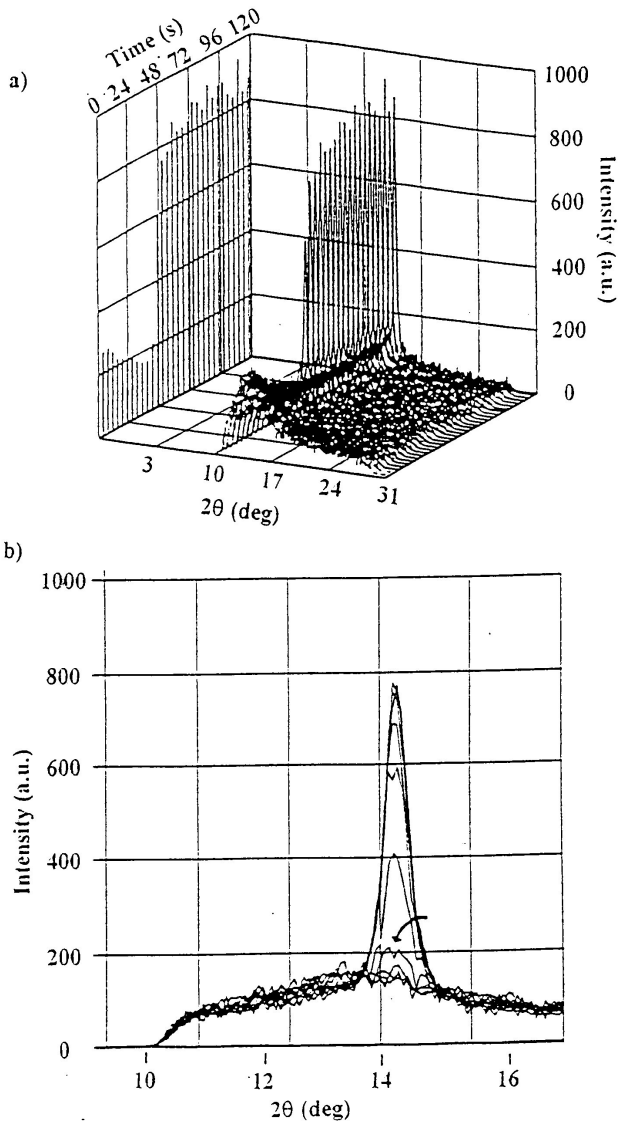

FIGURE 12. Results obtained using the Synchrotron radiation beam at LURE. a) The 3D graph shows the scattering intensity from the L-140 sample versus the scattering angle and for different time frames; the elongational rate $\dot{\varepsilon}_o$ was fixed to $0.047s^{-1}$. b) The same scattering curves are plotted in projection along the time axis in order to get some information on the width of the Bragg peak profile.

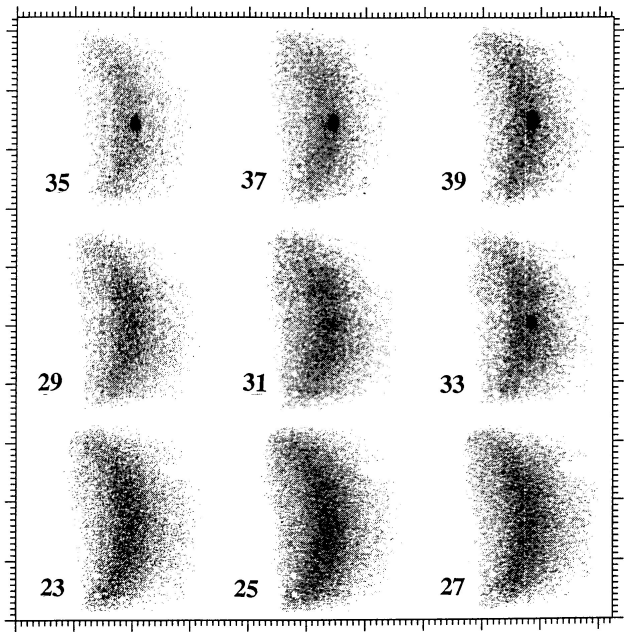

FIGURE 13. A series of 2-D X-ray scattering pattern recorded at the ESRF for B100 sample under an elongational rate $\dot{\varepsilon}_o = 0.029s^{-1}$. 9 Frames (3 second of acquisition time) have been selected around t_c, the time of the onset of crystallization (frame n° 31): the labels correspond to the numbering of the frames.

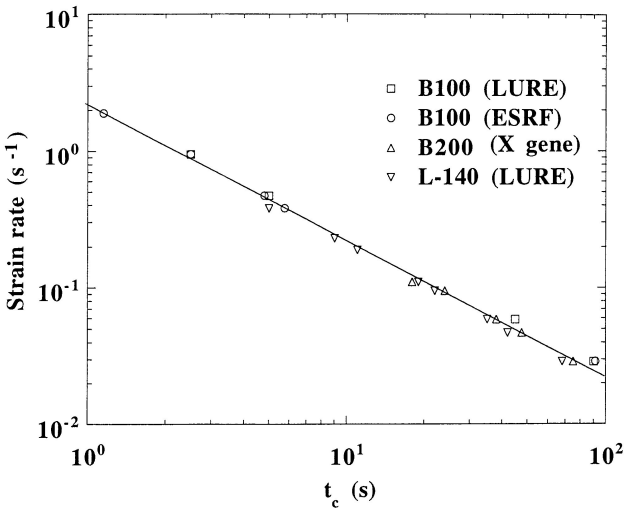

FIGURE 14. Deformation rate versus onset of crystallization (in seconds) for three samples B100 (○ LURE, △ ESRF), B200 (□ Classical X-ray generator) and L-140 (● LURE). The line has a slope equal to -1.

Bragg peak profile during the crystallization. It appears that the full width, at half maximum, which is related to the size of the crystallites remains constant as the peak grows.

Complementary experiments were performed at the ESRF with a better time resolution using the high brilliance beamline ID2 and a 2-D detector, synchronized with the traction machine. These experiments allowed us to achieve higher strain rates as shown in Fig. 13. Nine 2-D diffractograms for B100, before and after crystallization was determined with a time resolution of $0.2s$.

For the three samples, Fig. 14 shows the double plot of $\dot{\varepsilon}_o$ as a function of t_c the time of the onset of crystallization. All the points are aligned on a straight line of slope =-1 (almost two orders of magnitude), which demonstrates the inverse proportionality between t_c and $\dot{\varepsilon}_o$. The product $\dot{\varepsilon}_o t_c$ defined as the critical Hencky deformation $\dot{\varepsilon}_c$ is constant.

All theses results are also summarized in Table III. For L-140 we find $\dot{\varepsilon}_c = 2.0 \pm 0.1$ which correspond to $L/L_o \simeq 7$, for B200 we find $\dot{\varepsilon}_c = 2.2 \pm 0.1$ which correspond to $L/L_o \simeq 9$, while for B100 we find $\dot{\varepsilon}_c = 2.4 \pm 0.2$ which correspond to $L/L_o \simeq 10$. These averaged values do not reveal a systematic dependence on the molecular weight.

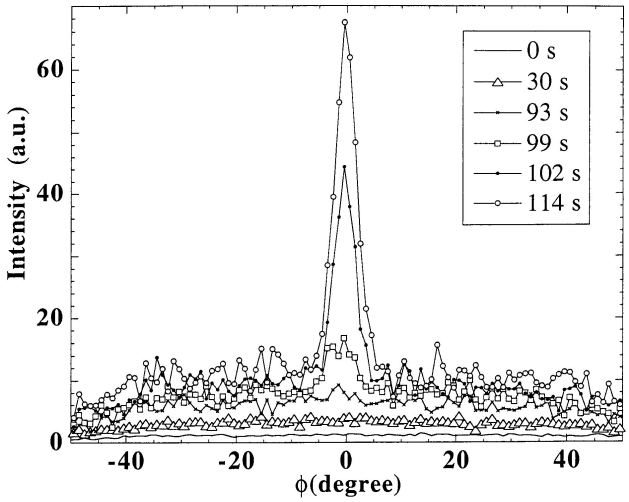

FIGURE 15. Averaged azimuthal distribution of the intensity along the ring at fixed $2\theta_{Bragg}$ for the B100 at $0.029s^{-1}$ and for different time frames (times are indicated in the legend).

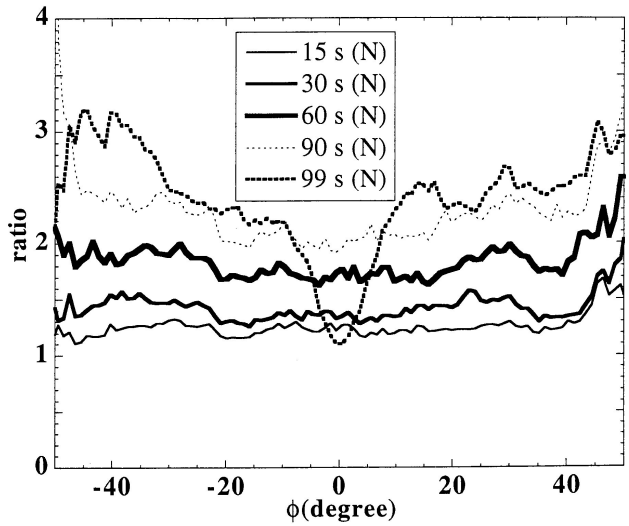

FIGURE 16. These curves show the ratio of the azimuthal intensities distribution for different frames (see legend) by the intensity of the initial one.

Figures 4 – 6 show the elongational viscosities which were recorded during the X-ray diffraction measurements. The arrows in the figures indicate the onset of crystallization t_c. It is clearly observed there exists a time delay between the anomalous strain hardening at t^* and t_c, which cannot be attributed to the poor accuracy in the time frame measurement. The values given in Table III indicate that the ratio $t^*/t_c(=\dot{\varepsilon}^*/\dot{\varepsilon}_c)$ is almost a constant independent of the strain rate $\dot{\varepsilon}_o$ and the molecular weight ($0.91 < \dot{\varepsilon}^*/\dot{\varepsilon}_c < 0.95$). This means that the strain hardening occurs when the elongation ratio L/L_o is around 80% of the value corresponding to the onset of crystallization.

From the time resolved diffraction measurements using either linear or area detectors, we can also analyze the lineshape of the diffraction peaks and its evolution during the crystallization process ($t > t_c$). As common in polymers, the full-width of the Bragg reflections $\Delta(2\theta)$ is controlled by the small coherent size L_c of the crystallites. According to the Scherrer expression,

$$\Delta(2\theta) = 0.9\lambda/L_c \cos\theta \tag{6}$$

One obtains for $\lambda = 1.54$ Å, and $\Delta(2\theta) = 0.4deg.$, a coherence length $L_c = 145$ Å (see Fig. 12b). From the evolution in the line width during the crystallization process one may thus analyze the possible growth of the crystallites. It is clearly visible that only the intensity of the Bragg peak increases without any change of its width ($\Delta(2\theta) = 0.4deg.$). This means that the crystallization scenario consists of continuous nucleation of new crystallites, each of them reaching its equilibrium size in a very short time. This result is confirmed over the full range of applied strain rates.

The data obtained with the area detector (Fig. 13) also show a high orientation of the crystal with the **c** axes along the stretching direction. In a first approximation the azimuthal width $\Delta\phi$ gives an upper limit for the width of the orientation distribution of the **c** axes around the stretching direction (see Fig. 15). We always observed $\Delta\phi < 5$ deg. The experimental configuration did not permit us to analyze accurately the azimuthal distribution of the diffuse scattering. Nevertheless by dividing the different azimuthal curve by the initial distribution corresponding to the isotropic amorphous state, we can notice a slight anisotropy of the scattering arising before the onset of crystallization (60 s – 90 s) as indicated in Fig. 16. This seems that the development of a slight anisotropy of the amorphous polymer occurs during the strain hardening between t^* and t_c.

Finally, from the ratio between the integrated intensity of the intense Bragg reflection and the integrated intensity of the diffuse amorphous scattering, we can estimate an order of magnitude for the maximum degree of crystallinity when the Bragg intensity levels off. It does not exceed 5%. Thus the stretched PIB might be compared to the stretched gel in which the crystallites play the role of cross links between chains and are responsible for the high (static) Young modulus observed after completion of the crystallization.

4. Conclusions

In two low molecular weight PIB samples studied, no crystallization and no anomalous strain hardening were observed under elongational flow conditions used. On the other hand higher molecular weight PIB samples exhibited both anomalous strain hardening at a critical Hencky deformation $\dot{\varepsilon}^*$ and crystallization at a deformation $\dot{\varepsilon}_c > \dot{\varepsilon}^*(2.0 < \dot{\varepsilon}_c < 2.4)$. At constant strain rate, the delay between t^* the time at which we observe a abrupt change in the strain hardening and t_c the onset of crystallization time remains difficult to evaluate due to a smooth change of slope in the elongational viscosity curves; however we were able to find that the ratio t^*/t_c is constant and equal to 0.93. The scattering experiments reveal that the size of the crystallites produced under stretching

does not change during the process, only the number of crystals increases up to a maximum degree of orientation of the growing crystalline phase in the poorly oriented amorphous phase. Nevertheless these results suggest that the strain hardening (corresponding to the anomalous flow) is highly correlated to the orientation of the polymer matrix between t_c and t^*, and further experiments are needed to confirm this aspect.

Acknowledgments

We wish to thank, Mrs. Helene Galliard and Mr. Didier Bleses (Laboratoire de Rheologie) for assisting in the design and manufacture of the traction machine. We are grateful to Mr. Guy d'Assenza (Laboratoire de Spectrometrie Physique) and also Mrs. Claudie Bourgaux (LURE) and Mr. Peter Bosecke (ESRF) for assisting in the processing of X-ray experiments.

∗ To whom correspondence should be addressed.

1. A.K. van der Vegt and P.P.A. Smit, *Adv. Polym. Sci. Technol.* **26** (1967) 313.
2. J.W.H. Kolnaar and A.J. Keller, *Non-Newtonian Fluid Mech.* **67** (1996) 213.
3. Brill and Halle, *Naturwissenschaften* **26** (1938) 12.
4. C.S. Fuller, C.J. Frosch, and N.R. Pape, *J. Chem. Phys.* **62** (1940) 1905.
5. T. Tanaka, Y. Chatani, and H. Tadokoro, *J. Polym. Sci. Polym. Phy. Ed* **12** (1974) 515.
6. G.L. Slonimsky, and A.A. Askadsky, *Mehanika Polymerov* **4** (1967) 659.
7. M.J.H. Koch, J. Bordas, E. Schola, H.C. and Broecker, *Polymer Bull* **1** (1979) 709.
8. A. Gonzalez-Alvarez, G. d'Assenza, J.F. Legrand, and J.M. Piau, *C. R. Acad. Sci. Paris* **320** (1995) 23.
9. J. Meissner, *International Workshop on Extensional Flows*, paper 4 (Mulhouse-La Bresse, 1983).
10. The transient shear viscosity has been determined independently using a Carrimed Weissenberg Rheometer.
11. N.E. Hudson, J. and Ferguson, *J. non-Newtonian Fluid Mech* **52** (1994) 105.
12. N. Willenbacher and R. Hingmann, *J. non-Newtonian Fluid Mech* **52** (1994) 163.
13. G.R. Mitchell, *"Comprehensive Polymer Science, vol IÓ* Eds. G. Allen, J.C. Bevington, C. Booth, and C. Pride (Pergamon Press, London, 1989) p. 687.